Influence of wind strength and direction on diffusive methane fluxes and atmospheric methane concentrations above the North Sea

Ingeborg Bussmann[1], Eric P. Achterberg[2], Holger Brix[3], Nicolas Brüggemann[4], Götz Flöser[3], Claudia Schütze[5], Philipp Fischer[2]

[1]Departments of Shelf Sea System Ecology & Coastal Ecology, Alfred-Wegener-Institut, Helmholtz Zentrum für Polar- und Meeresforschung, Kurpromenade 201, 27498 Helgoland, Germany

[2]GEOMAR, Helmholtz Centre for Ocean Research, Wischhofstr. 1-3, 24148 Kiel, Germany

[3]Helmholtz-Zentrum Hereon, Institute of Carbon Cycles, Max-Planck-Straße 1, 21502 Geesthacht, Germany

[4]Institute of Bio- and Geosciences – Agrosphere (IBG-3), Forschungszentrum Jülich GmbH, Wilhelm-Johnen-Str., 52425 Jülich, Germany

[5]Department of Monitoring and Exploration Technologies, Helmholtz Centre for Environmental Research - UFZ, Permoserstr. 15, 04318 Leipzig, Germany

correspondence to ingeborg.bussmann@awi.de

Abstract. Quantification of the diffusive methane fluxes between the coastal ocean and atmosphere is important to constrain the atmospheric methane budget. The determination of the fluxes in coastal waters is characterized by a high level of uncertainty. To improve the accuracy of the estimation of coastal methane fluxes, high temporal and spatial sampling frequencies of dissolved methane in seawater are required as well as the quantification of atmospheric methane concentrations, wind speed and wind direction above the ocean. In most cases, these atmospheric data are obtained from land-based atmospheric and meteorological monitoring stations in the vicinity of the coastal ocean methane observations.

In this study, we measured wind speed and direction as well as atmospheric methane directly on board three research vessels in the southern North Sea and compared the local and remote atmospheric and meteorological measurements on the quality of the flux data. In addition, we assessed the source of the atmospheric methane measured in the study area in the German Bight using airmass back trajectory assessments.

The choice of the wind speed data source had a strong impact on the flux calculations. Fluxes based on wind data from nearby weather stations amounted to only $58 \pm 34\%$ of values based on situ data. Using in-situ data, we calculated an average diffusive methane sea-to-air flux of 221 ± 351 µmol m^{-2} d^{-1} (n = 941) and 159 ± 444 µmol m^{-2} d^{-1} (n = 3028) for our study area in September 2019 and 2020, respectively. The area-weighted diffusive flux for the entire area of Helgoland Bay (3.78×10^9 m^2) was 836 ± 97 and 600 ± 111 kmol d^{-1} for September 2019 and 2020, respectively. Using the median value of the diffusive fluxes for these extrapolations resulted in much lower values, compared to area-weighted extrapolations or mean-based extrapolations.

In general, at high wind speeds, the surface water turbulence is enhanced and the diffusive flux increases. This enhanced methane input however is quickly diluted within the air mass. Hence, a significant correlation between the methane flux and the atmospheric concentration was observed only at wind speeds < 5 m s^{-1}.

The atmospheric methane concentration was mainly influenced by the wind direction, i.e., the origin of the transported air mass. Airmasses coming from industrial regions resulted in elevated atmospheric methane concentrations, while airmasses coming from the North Sea transported reduce methane levels. With our detailed study on the spatial distribution of methane fluxes we were able to provide a detailed and more realistic estimation of coastal methane fluxes.

1   Introduction

1.1   Necessity for coastal methane data

Methane (CH_4) is the second-most important greenhouse gas (GHG) after carbon dioxide (CO_2), accounting for 16–25% of atmospheric warming to date (Etminan et al., 2016). Aquatic ecosystems contribute 41% (median) or 53% (mean) of total global CH_4 emissions from anthropogenic and natural sources (Rosentreter et al., 2021a). Coastal seas are an important global source of GHGs (Saunois et al., 2020). For the open and coastal ocean including estuaries, Saunois et al. (2020) suggested an emission of 6 (range 2–10) Tg CH_4 yr^{-1}. A more recent study from Rosentreter suggested an emission of 8.4 (4.8–28.4, Q1-Q3) Tg CH_4 yr^{-1}, with a contribution of 3% from estuaries, 13% from tidal flats and 52% from continental shelves (Rosentreter et al., 2021a). The near-shore environments hence contribute the largest but most uncertain diffusive fluxes despite accounting for only ~3% of the global ocean area.

The reasons for the large range and uncertainty of coastal CH_4 fluxes are associated with the high spatial and temporal variability of fluxes in coastal ecosystems, driven by, for example, variations in tidal pumping and salinity gradients (Rosentreter et al., 2021a), exacerbated by a paucity of data with sufficient temporal and spatial resolution (Weber et al., 2019). Overall, aquatic GHG emissions are causing considerable uncertainty in global GHG assessments (IPCC, 2021). Thus, reducing the uncertainty in aquatic GHG budgets is important to allow improvements to biogeochemical models and climate predictions.

1.2   Traditional method for flux calculation

The air–sea gas flux is a function of the gas transfer velocity (k) and atmospheric and oceanic CH_4 concentrations (Wanninkhof, 2014, details see method section). Since k is difficult to measure, it is often parameterized using widely measured parameters such as wind speed. In offshore regions with greater water depth, wind is known as a good predictor for the gas transfer velocity because wind creates waves and currents which control turbulence and bubbles at the sea surface (Wanninkhof et al., 2009). Also in shallow waters, k can be well estimated by wind speed when the water depth is more than 10 m (Ho et al., 2018). Other techniques to determine k are eddy covariance measurements, tracer injection methods (Gutiérrez-Loza et al., 2022;Dobashi and Ho, 2023) and chamber measurements (Rosentreter et al., 2021b). The best way to determine k is an ongoing matter of debate.

Diffusive CH_4 fluxes are typically determined from direct surface ocean CH_4 observations and parametrizations of wind speed and atmospheric CH_4 concentrations. The atmospheric data used are normally taken from coastal

meteorological stations in close proximity to the marine observations (see for example (Myllykangas et al., 2020;Woszczyk and Schubert, 2021), or a combination of in-situ data and data obtained from a meteorological station is used (Mau et al., 2015;Bussmann et al., 2021b;Humborg et al., 2019). Other studies use in-situ data for all variables (de Groot et al., 2023: Thornton, 2016 #2655). We are not aware of any study on the influence of the data source on the quantification of diffusive CH_4 fluxes.

1.3 Atmospheric methane above a water body

The atmospheric CH_4 concentration is determined by several factors. One is the sea-to-air transfer through the diffusive CH_4 flux (Wanninkhof, 2014), implying that periods or areas with high diffusive CH_4 fluxes into the atmosphere would result in higher atmospheric CH_4 concentrations. However, there are contrasting reports in literature in marine science, with highest atmospheric CH_4 concentrations being observed during cruises with lowest CH_4 fluxes (Silyakova et al., 2020). Increasing atmospheric CH_4 levels were not found alongside enhanced dissolved CH_4 concentrations (Vogt et al., 2023;Law et al., 2010). These studies show that there is no clear mechanistic understanding of the relationship between dissolved CH_4 concentrations, CH_4 fluxes to the atmosphere and atmospheric CH_4 concentrations in shallow coastal water areas.

1.4 Methane in the North Sea

The CH_4 budget of the central North Sea is characterized by pockmarks (Römer et al., 2021), drilling activities (Vielstädte et al., 2017), and gas ebullition sites (Mau et al., 2015). In contrast, in the southern North Sea and areas close to the mainland, dissolved CH_4 mainly originates from autochthonous methanogenesis in sediments (Yin et al., 2019) with subsequent fluxes into the water column, and also from tidal flats ((Røy et al., 2008;Wu et al., 2015) and riverine inputs (Upstill-Goddard and Barnes, 2016). Borges et al. (2017) showed that warm summers in northern Europe in recent years have resulted in increased dissolved CH_4 concentrations due to enhanced methanogenesis, which has led to higher sea-to-air CH_4 fluxes along the Belgian coast (Borges et al., 2017;Borges et al., 2019).

Previous studies have investigated the temporal and spatial patterns of dissolved CH_4 between the German North Sea coast and the island of Helgoland (60 km offshore) on a monthly basis from 2010 to 2014 (Matousu et al., 2017;Osudar et al., 2015;Hackbusch et al., 2019). In these studies, the CH_4 concentrations near the coast ranged between 30 and 51 nmol L^{-1}, whereas near Helgoland, the concentrations were 14 ± 6 nmol L^{-1}. However, no flux data were calculated in these studies. At these high concentrations of dissolved CH_4 in the coastal North Sea (the equilibrium concentration is 2–3 nmol L^{-1}), the diffusive flux is mainly directed from the sea into the atmosphere.

1.5 Aim of study

The aim of this study was to establish the diffusive CH_4 fluxes from the sea into the atmosphere in the southern German Bight (North Sea) based on CH_4 concentration data of high spatial and temporal resolution. We also investigated the influence of the use of different auxiliary data sets on the calculation of the diffusive CH_4 fluxes over a wide area of the Helgoland Bay. We assessed whether increased diffusive CH_4 fluxes lead to detectable increases in atmospheric CH_4 concentrations and identified the atmospheric factors that influence CH4 concentrations in a given area.

2   Material & Methods

2.1   Study Sites

The cruises Stern-3 and 5 were performed in September 2019 and 2020, as part of the "Modular Observation Solutions for Earth Systems" (MOSES, (Weber et al., 2021)) subproject "Hydrological Extremes".

On Stern-3, the research vessels RV Littorina (German Helmholtz Centre GEOMAR), RV Ludwig Prandtl (German Helmholtz Centre Hereon) and RV Uthörn (German Helmholtz Centre AWI) left the harbor of Cuxhaven (Fig. 1) on 9 September 2019, heading for the island of Helgoland (German Bight) following different cruise tracks. On 10 September 2019, RV Littorina and Ludwig Prandtl returned to Cuxhaven and the Elbe Estuary, while RV Uthörn returned via the river Weser to Bremerhaven (Bussmann et al., 2020).

For Stern-5, the three research vessels started from Cuxhaven and the Elbe estuary on 30 August 2020, again heading for Helgoland (Fig. 2). In the following days, RV Littorina covered the area between Helgoland and Büsum (on the mainland), extending the cruise track towards the East. RV Ludwig Prandtl covered the area further north and west of the island of Amrum. Mya II (German Helmholtz Centre AWI) covered the area between Helgoland and Bremerhaven with the Weser Estuary. On the last day (3 September 2020) RV Mya II ended the cruise in Sylt, while the others returned to Cuxhaven (Bussmann et al., 2021a).
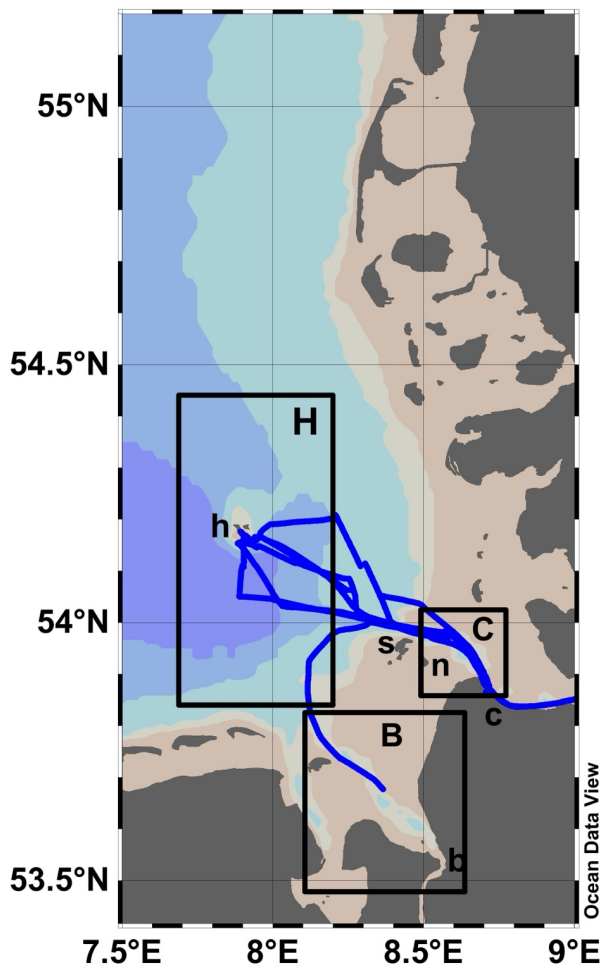
140 **Figure 1**. Cruise tracks for Stern 3, in September 2019 with RVs Littorina (blue), Ludwig Prandtl (green) and Uthörn (red). The areas for different flux calculations are also indicated: the area around Bremerhaven (B) with its meteorological station (b), the area around Cuxhaven (C) with its meteorological station (c) and the area around Helgoland (H) with its meteorological station (h). The islands Neuwerk (n) and Scharhörn (s) are also indicated.

145

Kommentiert [MOU1]: A corrected figure 1 was added, with the indications of the islands
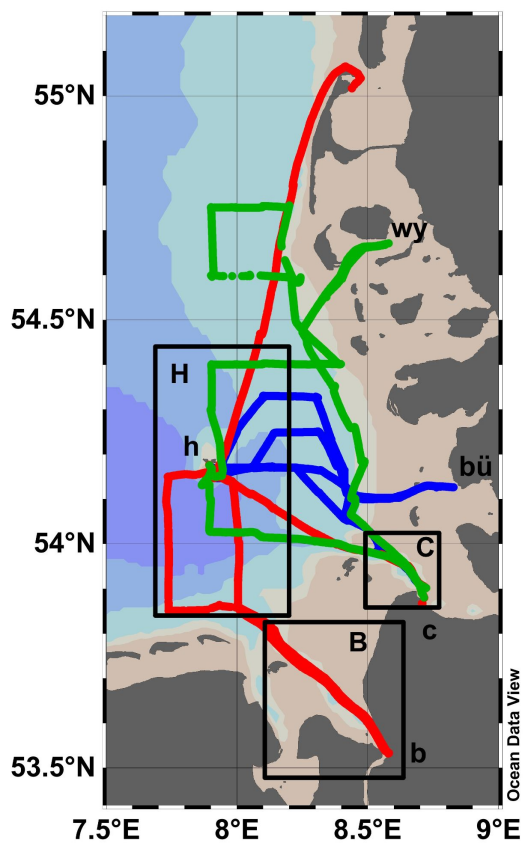
Figure 2. Cruise tracks for Stern 5, in September 2020 with RVs Littorina (blue), Ludwig Prandtl (green) and Mya II (red). The areas for different flux calculations are also indicated: the area around Bremerhaven (B) with its meteorological station (b), the area around Cuxhaven (C) with its meteorological station (c) and the area around Helgoland (H) with its meteorological station (h). The villages Büsum (bü) and Wyk auf Föhr (wy) are also indicated.

Kommentiert [MOU2]: A corrected figure 2 was added with the villages indicated.

2.2 Hydrographic and meteorological parameters

Basic hydrographic parameters, such as temperature, salinity, pH, oxygen, turbidity and chlorophyll fluorescence, were measured by shipboard measurement systems (FerryBoxes; 4Hjena, Germany) on all ships. FerryBox systems had been checked and calibrated during routine maintenance and in preparation for the cruises (Petersen, 2014). The water supply to the FerryBoxes and CH_4 analyzers (see below section Methane analysis) was taken from the ships' underway surface water supply (intake at 1–2 m). The water from the ship was either pumped through a flow-through basin with ambient air pressure (Stern-3) or from a specific in-situ pump tower (Stern-5) with a 10-l volume, pressure regulator and water overflow. Full details are in the cruise

reports (Bussmann et al., 2020;Bussmann et al., 2021a). Both systems ensured a constant and sufficient surface water supply to all sensors.

True wind speed and true wind direction were provided by the dship-system (nautical data system, Werum) or equivalent systems of Ludwig Prandtl, Mya and Uthörn (no data were available from RV Littorina) with a frequency of 1 min^{-1}. Available wind speed data were corrected to U_{10} (at 10 m height) with the respective measuring height (Touma, 1977):

$$U_{10} = U_{ship} (10 / z_{ship})^{0.143} \tag{1}$$

For any further calculations, we used the rolling mean over 10 minutes. For comparison, we also used wind data (hourly means) provided by the German Meteorological Service (https://cdc.dwd.de/portal/) for the weather stations Bremerhaven, Cuxhaven and Helgoland Dune. For each station, an area was set for which the respective wind data were used for the flux calculations (Fig. 1 and 2). Data on local tidal cycles were provided by the Bundesamt für Seeschifffahrt und Hydrographie (Federal Maritime and Hydrographic Agency, https://www.bsh.de/DE/DATEN/Vorhersagen/Gezeiten/gezeiten_node.html) for the sites Büsum and Wyk auf Föhr.

2.3 Methane Analysis

Dissolved CH_4 concentrations were measured with a dissolved gas extraction unit and a laser based analytical Greenhouse Gas Analyzer (GGA; both Los Gatos Research, United States) on all three ships. The degassing devices withdrew water from the flow-through units at 1.2 L min^{-1}. Methane was extracted from the water via a hydrophobic membrane and hydrocarbon-free carrier gas on the other side of the membrane (synthetic air or nitrogen, at 0.5 L min^{-1}). The carrier gas with the extracted CH_4 was then directed to the inlet of the gas analyzer. The time offset between the water intake and stable recording at the GGA was determined beforehand in the laboratory.

To convert the relative concentrations (ppm) given by the GGA to absolute concentrations (nmol L^{-1}), discrete water samples were obtained at least every hour. The CH_4 concentration in these bottles was determined using the headspace method and gas chromatographic analysis (Magen et al., 2014). Based on the obtained values, conversion factors (ppm to nmol L^{-1}) were determined for each setup. The regression lines and equations are given in the supplementary information (Fig. S1). Histograms for dissolved CH_4 concentrations are shown in figure S2. From the intercalibration stations (see section of data management) we calculated an instrumental error of 3.6%. To test the lower sensitivity of the set-up, aerated freshwater with an equilibrium concentration of 2.9 nM was measured in the laboratory and the instrument readings gave a concentration of 2.3 ± 0.3 nM.

For quality control, the regional boundaries were set to 1–500 nmol L^{-1} (see section data management). Atmospheric CH_4 was measured on board of the research vessels: for Stern-3 on the Littorina, Ludwig Prandtl and Uthörn with a Picarro G2301, a Picarro G2301, and a Microportable Greenhouse Gas Analyzer (LosGatos) respectively; for Stern-5 with a Picarro G2301, a Licor LI-8100A and another Picarro G2301, respectively. All data were corrected by the instruments for water vapor resulting in CH_4 dry values. The inlets for the instruments were approximately 4 m above the water surface and located either at the ship's bow (Littorina) or on a railing on the bridge (other ships). For quality control, the regional boundaries were set to 1.8–2.3 ppm (see

section data management). Additional data for atmospheric CH_4 concentration were obtained from the meteorological station in Mace Head, Ireland, (https://gml.noaa.gov/dv/data/index.php?site=MHD), using the

205   monthly means of September 2019 and September 2020 (1.942 ppm and 1.957 ppm, respectively).

2.4   Calculation of the diffusive methane flux

The overall gas exchange across an air–water interface was determined according to (Wanninkhof et al., 2009)

210   as:

$$F = k_{CH4} \cdot (c_m - c_{equ}) \tag{2}$$

where F is the rate of gas flux per unit area (mmol m^{-2} d^{-1}), c_m is the measured CH_4 concentration of the surface

215   waters, and c_{equ} is the atmospheric gas equilibrium concentration (Wiesenburg and Guinasso, 1979). For the atmospheric CH_4 concentration data, we either used our measured data or the data from the Mace Head observatory.

The gas exchange coefficient (k) is a function of water surface agitation. The k value in oceans and estuaries is determined mostly by wind speed (U_{10}). The determination of k is crucial to calculate the sea–air flux. We

220   calculated the gas exchange velocity k_{600} according to the following equation for coastal seas (Nightingale et al., 2000):

$$k_{600} = 0.333 U_{10} + 0.222 U_{10}^2 \tag{3}$$

225   We applied the wind-speed-based k_{600} parameterization from Nightingale et al. (2000) here largely because it is commonly used and represents a compromise between relationships that have a very strong or a very weak wind-speed dependence (Yang et al., 2019).

The calculated k_{600} (for CO_2 at 20°C) was converted to k_{CH4} (Striegl et al., 2012), and the Schmidt number (Sc) was adjusted based on water temperature and salinity (Wanninkhof, 2014):

230

$$k_{CH4} / k_{600} = (Sc_{CH4} / Sc_{CO2})^{-0.5} \tag{4}$$

To determine the influence of wind and atmospheric CH_4 on the flux calculation, three combinations of data sets were applied Table 1):

235   - Flux-1 with in-situ wind and in-situ atmospheric CH_4 concentrations, with a resolution of 1 minute.
- Flux-2 with in-situ wind but with the atmospheric CH_4 concentrations from the station Mace Head, Ireland, with a resolution of 1 month.
- Flux-3 fixed monthly atmospheric concentration from the station Mace Head and using hourly

240   wind data from the German Meteorological Service.

Table 1: Calculation of the diffusive CH_4 flux with several combinations of data sources.

	Flux 1	Flux 2	Flux 3
Dissolved CH_4	In situ*	In situ*	In situ*
Atmospheric CH_4	In situ*	Mace Head***	Mace Head***
Wind speed	In situ*	In situ*	DWD**

temporal resolution of every minute*, every hour**, every month***

245 To improve the estimation of the diffusive CH_4 flux for the whole study area, we calculated an area weighted diffusive flux. We split the diffusive flux data (flux-1 data, n = 941 for 2019 and 3028 for 2020) into groups with a bin size of 100 µmol m^{-2} d^{-1} and calculated a frequency distribution of the mean diffusive flux classes (0-100, 100-200, 200-300 ….. µmol m^{-2} d^{-1}). Next, the relative area was calculated by multiplying the relative frequency of each class with the total area. Then, the relative area of each class was multiplied with the

250 respective diffusive flux to obtain the relative areal flux. The sum of all relative areal fluxes finally resulted in the total weighted flux of the whole area. The standard deviation was determined from the relative areal fluxes. An example of the calculation is given in the supplementary Table S1.

To enhance the validity of our results, we extrapolated our calculated diffusive fluxes from our respective study

255 areas to areas in accordance with the ecosystem type classification of the German Federal Statistical Office (Statistisches Bundesamt ((Destatis), 2021), which assigns all areas of Germany to different ecosystem types without gaps or overlaps (https://oekosystematlas-ugr.destatis.de/). We used the following ecosystems, overlapping with our cruise track: eastern Wadden Sea of the Weser River (490000003), open coastal sea of the Weser (490000004), coastal sea of the Weser (490000005), Helgoland (590000002), coastal sea of the Elbe

260 River (590000003), western Wadden Sea of the Elbe (590000005), Outer Elbe North (590000006) and Piep Tidal basin (950000001, Fig. S3). These ecosystems cover a total area of 3.78 x 10^9 m^2 (377947 ha).

Note: "hat gelöscht: S1" appears in the margin as a tracked-change comment.

hat gelöscht: S1

2.5 Data management and handling

During the cruises or shortly afterwards, all data from all ships were uploaded to AWI's data web service

265 (Koppe et al., 2015), https://dashboard.awi.de/data-ingest/index.html#) at the highest available resolution. From this repository, data from different sensors can be combined, aggregated over time and downloaded as .csv files. In a second step, we applied a quality and plausibility control procedure to the data. In a first plausibility procedure, the ARGO algorithms (Bittig et al., 2019) for data quality flagging (manufacturer range, local range, spike check and gradient check) were applied assigning a bad data flag to values outside the ranges.

270 Additionally, as previous cruises had shown that it is essential to compare and possibly correct the sensor's data between the vessels (Bussmann et al., 2021b;Fischer et al., 2021), two, respectively four, intercalibration phases were scheduled during Stern-3 and Stern-5. During these phases, all vessels were in close proximity to each other (100–600 m) with all underway systems running and sampling the same water body.
In a machine-learning supported expert analysis (Fischer et al., 2021), sensor data of all three ships were first

275 visualized synoptically for the full time of the cruise and for the intercalibration intervals. From these comparisons, correction factors for those sensor data with significant accuracy deviations during the intercalibration phases were calculated and applied to the ships' respective sensor data. For example, on Stern-5, the water temperature from Littorina was used as a lead sensor as confirmed by precise measurements. As the

280 temperature data from RV Ludwig Prandtl deviated by -0.03° during the intercalibration phases, +0.03°C were added to those temperature data. In contrast, the temperature data from RV Mya deviated for about + 0.07° from the reference value (from Littorina), therefore -0.07° were subtracted from RV Mya's temperature data. For subsequent calculations, all data were used with one minute resolution.

All calculations and statistics were performed with R-studio (version 2023.09.01+494, Posit Software, PBC).

285 The combined and corrected datasets, including the details of correction, can be found at the online repository pangea.de (https://doi.pangaea.de/10.1594/PANGAEA.962691 for Stern-5, and https://doi.org/10.1594/PANGAEA.964319 for Stern-3).

hat gelöscht: ##

hat gelöscht: , submitted

290 **3 Results**

3.1 Oceanographic and meteorological conditions in September 2019 (Stern-3)

Water temperatures in the study area in September 2019 ranged from 17.1 to 19.7°C, salinity ranged from 18.6 to 33.1, and oxygen saturation ranged from 80.1 to 100.4%. The meteorological situation differed substantially between 10 and 11 September, with a mean wind speed of 6.7 $\pm$ 2.9 m s^{-1} compared to 9.2 $\pm$ 2.9 m s^{-1}, and the

hat gelöscht: and the

295 wind direction shifted from west and west-northwest to southwest, respectively (Fig. 3).
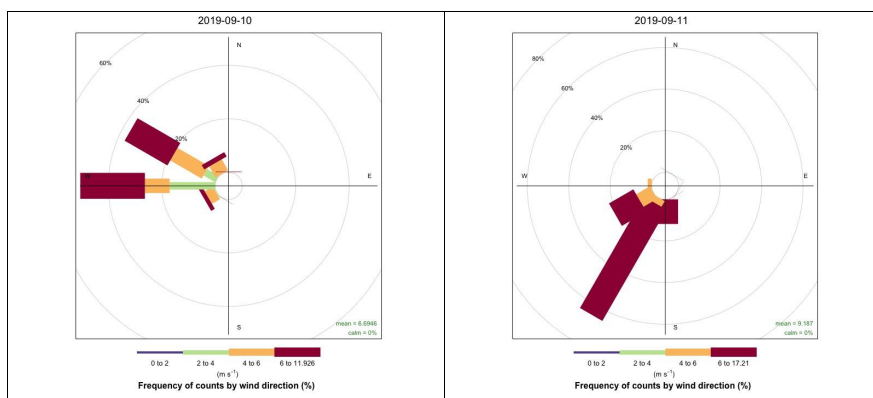
Fig. 3 Wind rose with wind speed and direction for 10 September (left) and 11 September 2019 (right, Stern-3).

As the diffusive flux was calculated using the wind speed data, the CH$_4$ related parameters are also described

300 separately for the two days. On 10 September, dissolved CH$_4$ concentrations showed a median of 22.6 nmol L^{-1} (range 3.9–304.9 nmol L^{-1}). High CH$_4$ concentrations were encountered near Cuxhaven, and at two to three patches between Helgoland and Cuxhaven (Fig. 4). On 11 September, concentrations were lower, with a median of 12.3 nmol L^{-1} (range 1.1–175.8 nmol L^{-1}). Lowest concentrations (1–2 nmol L^{-1}) were encountered west of the islands of Scharhörn and Neuwerk.

305 Atmospheric CH$_4$ concentrations had a median of 1.949 ppm (range 1.936 to 1.971ppm) on 10 September versus a median of 2.064 ppm on 11 September (range 1.948–2.255 ppm). On 11 September, rather high values (2.15 ppm) were observed near the island of Scharhörn. As the atmospheric CO$_2$ data were not elevated at this site, the influence of ship exhausts can be excluded. The wind was coming from south-southwest (200°), and the

tide was just increasing. We assume that the air mass crossing our cruise track had an inherent natural variability.

The diffusive flux was first calculated with in-situ wind and in-situ atmospheric CH$_4$ concentrations (flux-1, flux-2 and flux-3 data are shown in Table 2 and described in section 3.3). For both days combined, the average flux was 221 ± 351 µmol m^{-2} d^{-1}, the median was 97 µmol m^{-2} d^{-1}, and the range was from -27 to 2342 µmol m^{-2} d^{-1}. On 10 September, the diffusive flux had a median of 131 µmol m^{-2} d^{-1} (range 316–1500 µmol m^{-2} d^{-1}), with lowest values near Helgoland and near the island of Scharhörn (Fig. 4, left). Highest values were observed southeast of Helgoland. On 11 September, the diffusive flux was half of the one on the day before with a median of 62 µmol m^{-2} d^{-1} (range -27 – 2342 µmol m^{-2} d^{-1}). Highest values were observed again in the region between Helgoland and Cuxhaven; lowest and negative values were observed west of Cuxhaven (Fig. 4 right).
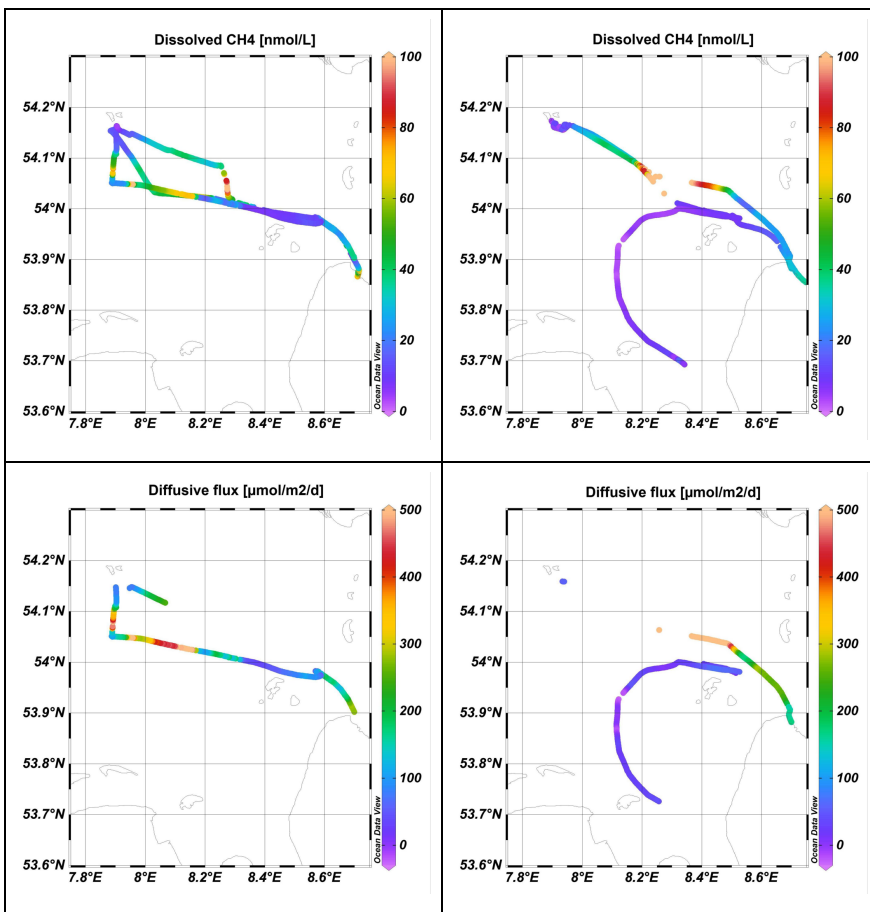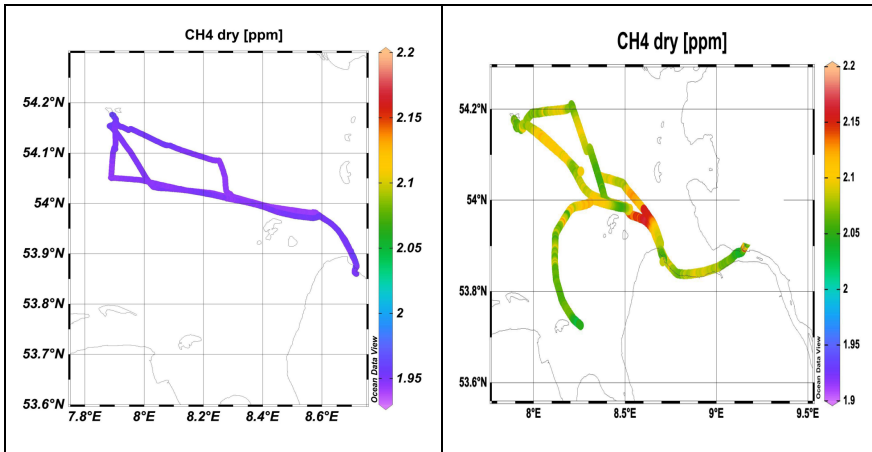
Fig. 4: Concentrations of dissolved CH₄ (top), diffusive CH₄ flux (middle) and in-situ atmospheric CH₄ concentrations (bottom) on 10 September (left) and 11 September (right).

325

3.2   Oceanographic and meteorological conditions in September 2020 (Stern-5)

Water temperatures in the study area in September 2020 were warmer compared to 2019, ranging from 17.6 to 21.4°C, salinity ranged from 13.8 to 33.4 and oxygen saturation ranged from 70 to 109%.

The meteorological situation differed substantially between the sampling dates, and therefore the data are presented per day (and not for the whole area). On 31 August, the mean wind speed was 2.6 ± 2.2 m s⁻¹ coming from the north-northwest. On 1 September, the wind direction shifted towards northeast, with a mean speed of 4.5 ± 1.9 m s⁻¹. On 2 September, wind speed decreased to 2.3 ± 1.4 m s⁻¹ with no preferred direction. On 3 September, the wind freshened to a mean of 7.6 ± 3.7 m s⁻¹ and was blowing from the south and south-southwest (Fig. 5).

335
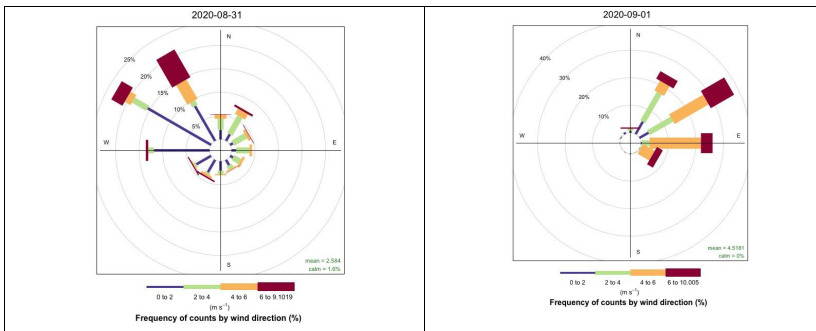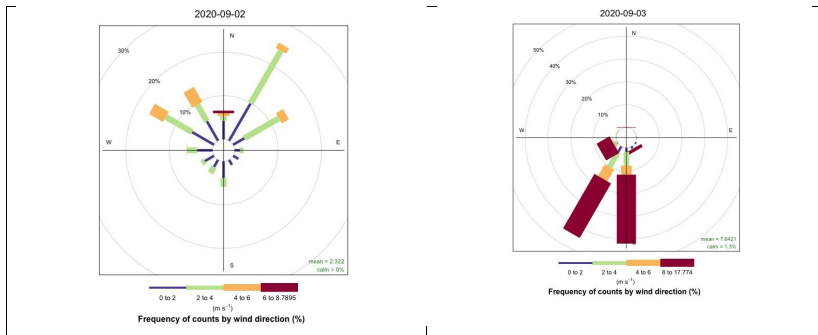
Figure 5: Wind rose with wind speed and direction for 31 August to 3 September 2020 (Stern-5).

345 Dissolved CH₄ concentrations for all days ranged from 1.4 to 607.9 nmol L^{-1}, with a median of 26.2 nmol L^{-1} (Fig. 6 left). Low concentrations of dissolved CH₄ (5–10 nmol L^{-1}) were observed southwest of Helgoland, in the outer Weser Estuary and in the northern region of the study area towards the island of Sylt (Fig. 6a). West of Büsum, we observed an area of high concentrations, as well as near Amrum, i.e., near the North Frisian Wadden Sea (> 100 nmol L^{-1}), with additional patches of elevated concentrations (70–100 nmol L^{-1}) located, for

350 example, east and north of Helgoland.

The average diffusive CH₄ flux (flux-1) was 159 ± 444 μmol m^{-2} d^{-1} (flux-2 and flux-3 data are shown in Table 2 and described in section 3.3). The median diffusive CH₄ flux for all days combined was 61 μmol m^{-2} d^{-1}, ranging from 0.2–4645 μmol m^{-2} d^{-1}. The spatial distribution of the flux was mostly a mirror image of the dissolved CH₄ concentration (Fig. 6 right). For the dataset from RV Littorina no flux data were calculated, as no

355 wind data were available. The data for dissolved and atmospheric CH₄ and the diffusive CH₄ flux for the individual days are shown in Figure S4, analogous to Fig. 4.

hat gelöscht: S2
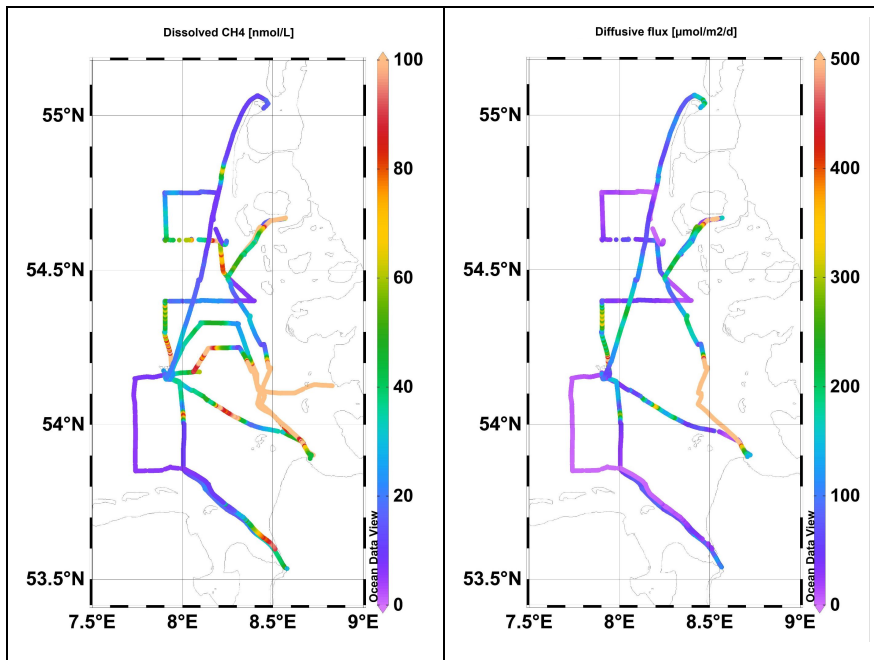
Figure 6: Concentrations of dissolved CH₄ (left) and the diffusive CH₄ flux (right) for the whole study area and Stern-5 study period (31 August to 3 September 2020).

360

hat gelöscht: 30
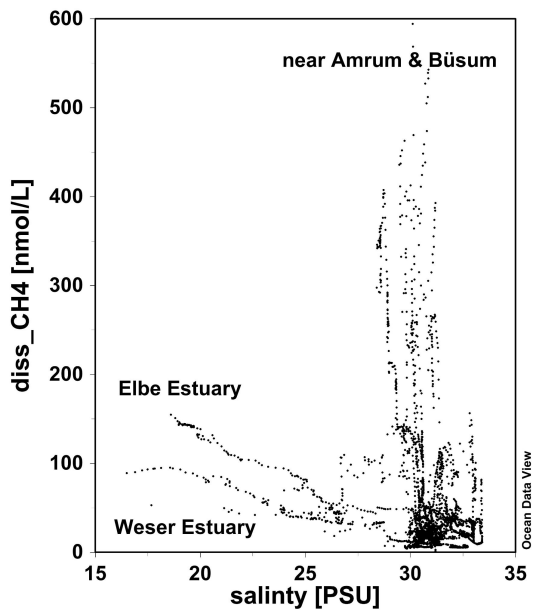
Fig. 7: Dissolved CH4 **concentration plotted versus salinity for September 2020 (Stern-5). The geographic location of the data pairs is also indicated.**

In both the Weser and Elbe estuaries, methane-rich river water was diluted with methane-poor marine waters (Fig. 7). The riverine endmember of the Weser showed lower CH_4 concentrations (95 nmol L^{-1}) than the Elbe endmember (151 nmol L^{-1}). However, highest CH_4 concentrations coincided with high salinities (> 30). These concentrations were all observed in the area west of Amrum and Büsum in the Wadden Sea. Thus, these areas were clearly not part of the dilution scheme, but a strong source of CH_4.

The median atmospheric CH_4 concentrations increased during the observed time span, from 1.951 ppm on 31 August, 1.979 ppm on 1 September, 2.022 ppm on 2 September to 2.078 ppm on 3 September (Fig 8). This increase over time was especially evident when comparing 1 and 2 September. The same area was covered (as the ships were returning to the same ports), and a substantial increase was observed, especially near the coast.
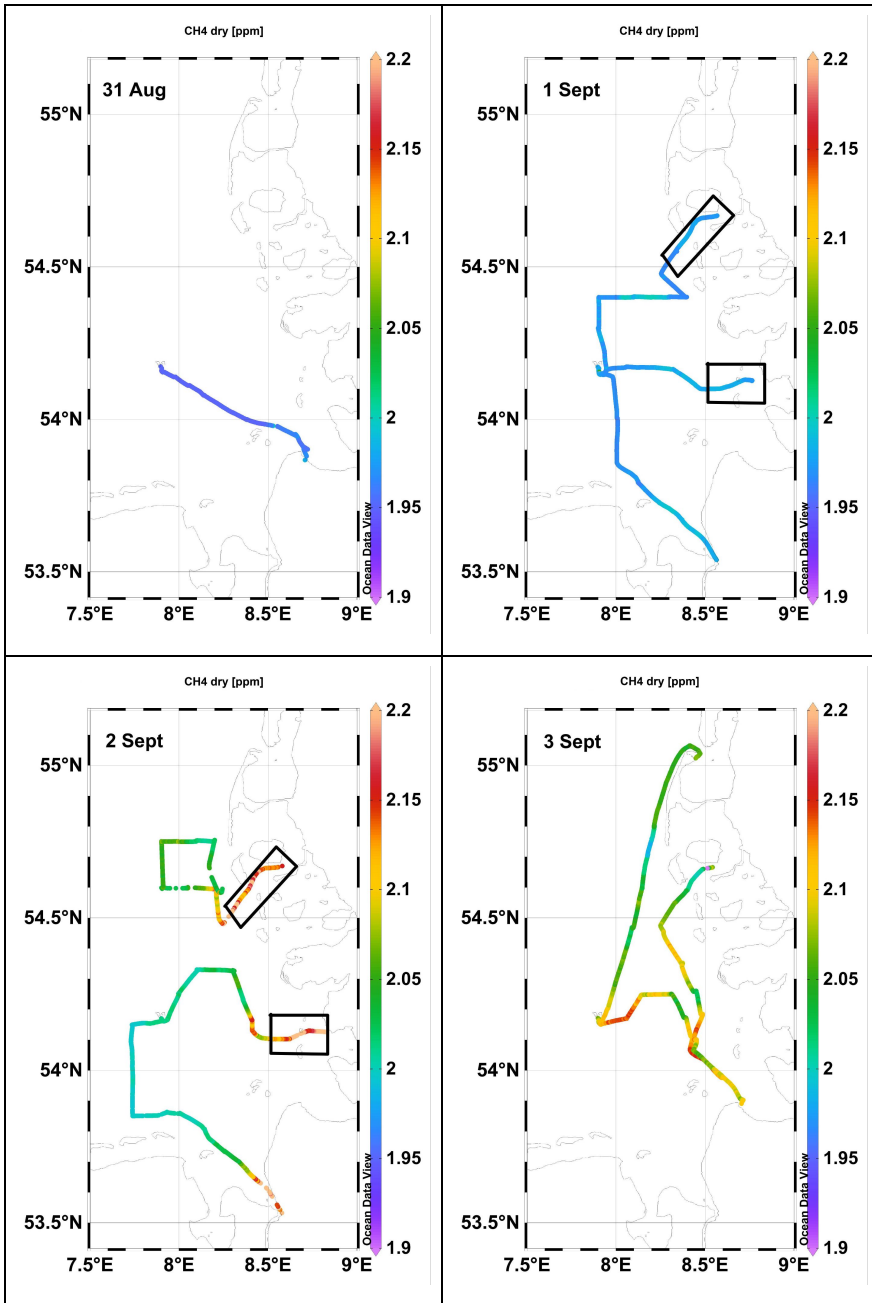
Figure 8: Atmospheric CH$_4$ concentration for 31 August to 3 September 2020 (Stern-5). The black boxes mark the areas where the vessels approached or left the Wadden Sea area.

385 **3.3   Calculations of diffusive fluxes using in-situ and land station-based data**

The calculation of the diffusive CH$_4$ flux was performed with three combinations of datasets to explore the influence that the use of atmospheric background data (for CH$_4$) and the closest land stations (for wind) has on CH$_4$ flux results (Table 1). For a better assignment of the wind data, the area was split into three boxes, one near Helgoland, one near Bremerhaven and one near Cuxhaven (see Fig. 1 and 2).

390 For the September 2019 cruises, the median in-situ atmospheric CH$_4$ concentrations ranged from 1.950 to 2.060 ppm, compared to a monthly mean of 1.942 ppm at the Station Mace Head (Table 2). For the wind speed, there was no or only a small difference between the in-situ data and data from the weather stations in Bremerhaven and Helgoland, while for the station Cuxhaven wind speed was almost 4 m s^{-1} lower than the in-situ wind speed. Higher atmospheric CH$_4$ concentrations lead to higher equilibrium concentrations of dissolved CH$_4$, and

395 therewith to a smaller oversaturation and lower diffusive fluxes. In 2019, the measured atmospheric CH$_4$ concentrations were always higher than those at the meteorological station. Consequently, the flux-2 values were often slightly higher than the flux 1 values (Fig. S5). The strongest difference was noticeable when comparing flux-1 with flux-3. When station data were used for both atmospheric CH$_4$ and wind (flux-3), there were substantial differences from the calculations using only in-situ data (flux-1).

400 The median in-situ atmospheric CH$_4$, concentrations ranged from 1.967 to 1.994 ppm for the September 2020 cruises, encompassing the monthly mean of 1.987 ppm at the Station Mace Head (Table 2). The wind speed measured on board the vessels was always higher than the data from the stations, with a difference of 0.4 and 0.5 m s^{-1} for Bremerhaven and Cuxhaven, and a difference of 0.8 m s^{-1} for Helgoland, resulting in comparatively lower flux-3 data. The flux-1 and flux-2 data were similar or almost identical, while flux-3 data were clearly

405 different or lower than the other two fluxes (Fig. 9). For both years, the number of flux-3 data was higher than for flux-1 and flux-2. The wind data for flux-3 were taken from the meteorological station with hourly averages, while the in-situ wind data were measured every minute, but with data gaps due to the quality control of the data.

410

Table 2: The median concentrations of dissolved and atmospheric CH$_4$ and median wind speed in September 2019

415 **and September 2020, calculated either with in-situ data, with monthly mean data from Station Mace Head for atmospheric CH$_4$ or as hourly mean wind data from three weather stations at Bremerhaven, Cuxhaven and Helgoland. The calculation of the diffusive flux was performed according to Table 1. The flux calculations were performed for an area near Bremerhaven (area B), an area near Cuxhaven (area C) and an area near Helgoland (area H), see also Figures 1 and 2.**

420

	Dissolved CH$_4$ in situ	Atmospheric CH$_4$ in situ / Mace Head	Wind speed in situ / meteo. station	Flux-1	Flux-2	Flux-3
	nmol L^{-1}	ppm	m s^{-1}	μmol m^{-2} d^{-1}		
2019	median	median	median	mean ± SD (n)		
Area B	8.0	2.060 / 1.942	9.5 / 9.5	32 ± 4; (51)	36 ± 8; (64)	38 ± 15; (65)
Area C	14.2	1.950 / 1.942	10.4 / 6.5	138 ± 78; (227)	142 ± 78; (293)	50 ± 25; (493)
Area H	24.1	1.956 / 1.942	7.5 / 7.5	184 ± 192; (281)	185 ± 190; (281)	105 ± 88; (514)
2020						
Area B	22.6	1.994 / 1.957	3.2 / 2.7	52 ± 36; (269)	52 ± 36; (282)	23 ± 17; (269)
Area C	79.6	1.967 / 1.957	2.7 / 2.3	235 ± 342; (226)	235 ± 342; (226)	57 ± 38; (244)
Area H	26.4	1.991 / 1.957	5.9 / 5.1	88 ± 92; (827)	90 ± 92; (851)	57 ± 62; (1186)

425
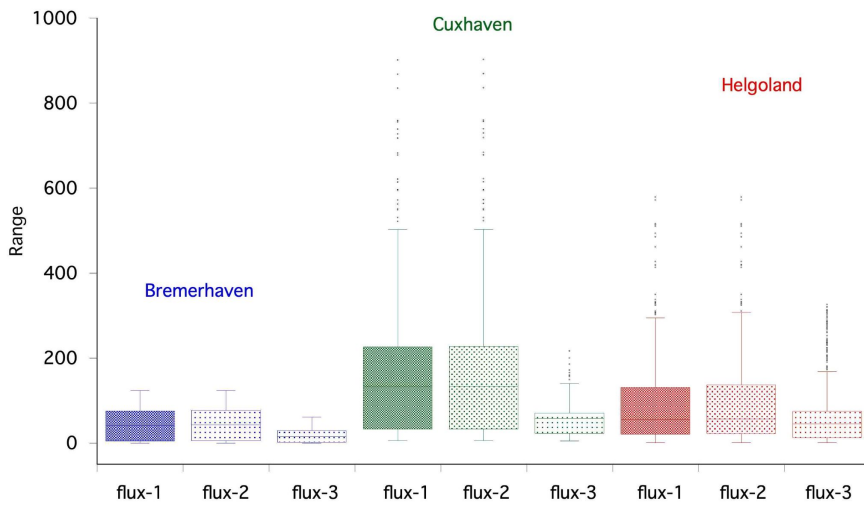
Figure 9: Range of diffusive CH$_4$ fluxes calculated with all in-situ data from the cruises in September 2020 (flux-1), with in-situ data and atmospheric CH$_4$ data from the land station (flux-2), and with in-situ data and atmospheric CH$_4$ concentration and wind from three land stations (flux-3). The calculations were performed for the region of
430 **Bremerhaven (blue), for Cuxhaven (green) and Helgoland (red, see Fig. 2)**

3.4   Area-weighted calculation of the diffusive methane flux

The frequency distribution for the 2019 flux data is shown in Fig. S6. The majority of flux data (48%) belonged to the range class 0–100 μmol m^{-2} d^{-1}. The subsequent classes (100–500 μmol m^{-2} d^{-1}) had frequencies of 40% in

hat gelöscht: S4

hat gelöscht:

total. Fluxes higher than 500 μmol m^{-2} d^{-1} had a total frequency of 9%. Negative fluxes (-100–0 μmol m^{-2} d^{-1}) occurred with a frequency of 3%.

The frequency distribution for the 2020 flux data is shown in Fig. S7. Again, most of the data were found in the class 0–100 μmol m^{-2} d^{-1}, with a frequency of 67%. The next class 100 – 200 had a frequency of 21%; the classes 200-300, 300-400 and 400-500 had a total frequency of 7%. Fluxes higher than 500 μmol m^{-2} d^{-1} had a total frequency of 5%. In contrast to the September 2019 values, negative fluxes (in the range of -100–0 μmol m^{-2} d^{-1}) were not observed.

445   To calculate the weighted flux for our study area, we related the total area of the Helgoland Bay (3.78 x 10^9 m^2) to the frequency of the flux classes, as explained in the Method section and in supplementary Table S1. This resulted in the total area-weighted diffusive fluxes of 836 ± 32 and 600 ± 21 kmol d^{-1} for the area of Helgoland Bay for 2019 and 2020, respectively.

The other approach was to multiply the median or mean of all flux data with the total area. The standard
450   deviation for the mean was also multiplied with the area to maintain the same unit. This resulted in much lower values for the median flux data and identical values for the mean flux data, compared to the area-weighted approach. However, the standard deviation of the mean flux data was much larger than for the area-weighted approach (Table 3).

455   **Table 3. Comparison of three approaches to calculate the total diffusive flux from Helgoland Bay with an area of 3.78 x 10^9 m^2 based on the median, mean or area-weighted diffusive flux.**

	Area related diffusive flux in Helgoland Bay (kmol/d)		
	median (range)	mean ± SD	Area-weighted
Sept 2019	365 (-104–8851)	836 ± 1328	836 ± 32
Sept 2020	229 (1–17558)	600 ± 1676	600 ± 21

3.5   Estimation of flux contributions to atmospheric concentrations

We often observed a substantial increase in atmospheric CH$_4$ concentration between single days, but the source
460   of the additional atmospheric CH$_4$ was unclear. Sources could be the diffusive flux from the sea into the atmosphere or different origins of the air masses above the water.

In September 2019, we observed an increase in atmospheric CH$_4$ concentrations of 0.116 ppm between 10 and 11 September (from 1.950 to 2.065 ppm). The average diffusive flux on these two days was 222 μmol m^{-2} d^{-1}. Using the ideal gas law, we converted the CH$_4$ flux into a gas volume (air temperature of 16°C, pressure of 1015
465   mbar, time frame one day, comparable to the calculations of (Zang et al., 2020). Under the idealized assumption that we had no advective exchange, the diffusive flux alone would explain the observed concentration difference for a mixed atmospheric layer of 45 m in height.

In September 2020, the strongest difference in atmospheric CH_4 was observed between 1 and 2 September (delta = 0.079 ppm). The average diffusive flux for these two days was 48 µmol m^{-2} d^{-1}. The calculation for the idealized mixed layer height for this day yielded 15 m. Further assuming a planetary boundary layer height for mid-latitudes of about 300 m (a lower range estimate based on climatologies by (Ao et al., 2012) and a well-mixed surface layer of about 10% thereof, i.e., 30 m, the observed increase of atmospheric CH_4 in September 2019 could have been mainly due to diffusive flux from the sea into the atmosphere. In September 2020, however, the calculated height of the mixed surface layer would be 15 m, which is not realistic. Thus, the observed increase of atmospheric CH_4 has to be attributed mainly to advection.

A linear regression analysis between the diffusive flux and atmospheric CH_4 revealed no significant correlation; also, when split by single dates. Strong wind results in an increased diffusive flux, but as the mixing of the atmospheric CH_4 also increases, the signal of the diffusive CH_4 imported will be "diluted". Thus, we tested the hypothesis that only under low wind conditions a correlation would be detectable. Therefore, we split the wind in classes (<10, <9, <8 m s^{-1} etc.) and repeated the analyses for each class. These class-separated calculations revealed no correlation between the diffusive flux and atmospheric CH_4 concentration at wind speeds >5 m s^{-1}. However, at wind speeds less than 5 m s^{-1}, a significant correlation between diffusive flux and atmospheric CH_4 was detected ($r^2 = 0.52$). The strongest correlation was detected at wind speeds <2 m s^{-1} ($r^2 = 0.75$).

A further possible cause for increases in atmospheric CH_4 concentrations are changes in advection under the assumption that wind coming across the sea has a lower CH_4 content than wind coming from land. As wind direction is no linear parameter, we divided the parameter into 30° classes, followed by a one-way analysis of variance. It revealed that the wind direction had a significant influence on the atmospheric CH_4 concentrations in our two study periods of September 2019 and September 2020 ($p < 0.001$).

In September 2019, the highest atmospheric CH_4 concentrations were observed when the wind came from the south-southwest (210–240°) with a median of 2.08 ppm, and lowest values were observed when the wind came from northerly directions (0–30°, 300–330°, 330–360°) with a median of 1.94 ppm, 1.95 ppm and 1.95 ppm, respectively. In September 2020, highest atmospheric CH_4 concentrations were observed when the wind came from the south (180–210°) with a median of 2.07 ppm, and lowest values were observed when the wind came from the east (90–120°) with a median of 1.98 ppm.

In addition to the wind signal, we looked for a possible tidal impact. On 1 September 2020, the RV Ludwig Prandtl approached the harbor at Wyk auf Föhr from 14:00–16:00 UTC and left port around 04:00–06:00 UTC the following morning (Fig. 8). The wind was blowing from northeast on both occasions, with rather low wind speed of less than 5 m s^{-1} (Fig. 5). High concentrations of dissolved CH_4 were observed, during the approach of the harbor (the data points outside the dilution scheme of Fig. 7). The diffusive CH_4 flux increased, and a most pronounced increase of 0.186 ppm of atmospheric CH_4 was observed (Table 4). In contrast to the overall analyses described above, for this areal section neither wind speed nor diffusive flux were correlated with atmospheric CH_4. However, as Wyk auf Föhr is surrounded by the tidal flats of the Wadden Sea, at low tide these flats are exposed to the atmosphere and tidal creeks withdraw pore water from the surroundings, which results in increased atmospheric CH_4 due to the release of CH_4 formed through anaerobic processes. A similar pattern of atmospheric CH_4 was observed for the tidal area off Büsum in the cruise section covered by RV Littorina. Atmospheric CH_4 increased for this section from 1.975 to 2.193 ppm, however no additional data (wind, diffusive CH_4 flux) are available for this ship.

Table 4: Atmospheric CH4 concentration in relation to tidal state, wind and diffusive CH4 flux.

Section toward Wyk/Föhr	1 September 2020 14:00–16:00 UTC	2 September 2020 04:00–06:00 UTC
Atmospheric CH$_4$ (ppm)	1.971 ±0.007	2.157 ± 0.04
Diffusive flux (µmol m^{-2} d^{-1})	24 ± 15.9	115 ± 22
Wind speed (m s^{-1})	4.6 ± 0.5	3.1 ± 0.4
Wind direction (°)	63 ± 4	44 ±12
Tide at Wyk	HT at 12:39	LT at 07:28
Section towards Büsum	1 September 2020 10:40–11:40 UTC	2 September 2020 04:40–05:40 UTC
Atmospheric CH$_4$ (ppm)	1.982 ±0.0072	2.140 ± 0.02
Tide at Büsum	HT at 11:24	LT at 05:53

515

4 Discussion

4.1 Error discussion for calculations of diffusive fluxes using different source data

The calculation of the diffusive sea-air flux depends very much on the parametrization of k. The most frequently used formula is the one from Wanninkhof 2014. For comparison we applied this formula to our data set from 2020; and average flux was very similar 153 ± 441 µmol m^{-2} d^{-1} according to Wanninkhof versus 159 ± 444 µmol m^{-2} d^{-1} according to Nightingale. Both parametrizations should provide good estimates for most insoluble gases at intermediate wind speed ranges (3-15 m s–1). Our wind data ranged from 1 – 11 m/sec. The study of (Ho et al., 2018) concludes that if the mean depth of the water body is greater than 10 m, an ocean wind speed/gas exchange parameterization could be used in such environments. The mean water depth in our study area 19 ± 12 m in 2019 and 17 ± 13 m in 2020. We therefore believe that the parametrization of Nightingale is appropriate for our study area. However, it should be kept in mind that also this parametrization holds an uncertainty of 19%. Other factors influencing the parametrization of k are rain (which did not occur during our cruises), water-side convection, and a biological surfactant suppression term (Gutiérrez-Loza et al., 2021). During summer, convection and surfactants seemed to act as competing mechanisms controlling the flux. Convective processes slightly enhanced the downward flux, while surfactants tended to suppress it (Gutiérrez-Loza et al., 2021).

In this study we applied several different methods to calculate diffusive sea-to-air CH$_4$ fluxes, either by using different databases for local values or by applying a weighted method for CH$_4$ fluxes for larger areas. The comparison between results obtained using different data sources showed that the choice between using atmospheric CH$_4$ concentrations from in-situ data or from a land station had no large effect (flux-1 versus flux-2, Fig. 9). In our study, the monthly average atmospheric CH$_4$ concentration from Mace Head station, that is usually used for providing atmospheric background concentrations, always showed lower values than our in-situ

540   data. Thus, the saturation concentration of dissolved CH_4 was lower, resulting in a smaller sea-to-air diffusive flux. However, in relation to the variability of the measured datasets, this difference was minor. The calculated flux-2 values reached on average $103 \pm 6\%$ of the corresponding flux-1 values (n = 6).

In contrast, it was important to use the in-situ wind speed for calculating the CH_4 fluxes (flux-3) instead of using data from the closest meteorological land stations. In some cases, the wind data were nearly identical, in other
545   cases the wind data from the land monitoring stations were lower, resulting in significantly smaller diffusive fluxes. The stronger impact of the wind speed is based on the fact that the flux calculation uses a quadratic wind speed formulation (equation 2, (Nightingale et al., 2000). Relating the flux-3 (land station) data to the flux-1 (in-situ) data revealed that the flux-3 values only reached an average of $58\% \pm 34\%$ of the flux-1 values (n = 6). As our flux data have a high variability (see below), a high temporal resolution of the data (as in flux-1) is favorable
550   over hourly (wind data) or monthly (atmospheric CH_4 data) resolution. Several combinations of in-situ data and data from databases have been reported in literature for calculating diffusive sea-to-air CH_4 fluxes (Myllykangas et al., 2020;Woszczyk and Schubert, 2021;Mau et al., 2015;Bussmann et al., 2021b;Humborg et al., 2019). Based on our direct comparison of these different approaches, we strongly recommend obtaining in-situ wind data.
555   We furthermore observed a high variability in all diffusive CH_4 flux data. For the entire 2019 dataset, the average diffuse CH_4 flux was 221 ± 351 µmol m^{-2} d^{-1} (n = 941), and for 2020 it was 159 ± 444 µmol m^{-2} d^{-1} (n = 3028). The coefficient of variation (CV) was 158% and 279%, respectively. Flux values for CH_4 in general have a high variability (36-71% (de Groot et al., 2023); 73% (Bussmann et al., 2021b), 78% (Humborg et al., 2019)), so that the CV values found here are not unusual. However, to avoid a possible elevated flux variability due to a
560   low sample size (methodological error), we applied a modified bootstrap analysis on the 2020 data to elucidate the effect of sample size on the calculated flux variability. The 2020 dataset had a total of 3028 measurements. From this dataset, we iteratively drew random subsamples, beginning with 20 values and increasing the sample size by 10 and 100 in each iteration. By this method, we finally received 39 datasets with an increasing number of flux values, starting at 20 and reaching up to 3028 values. The mean of these 39 datasets was calculated and
565   plotted versus sample size (Fig. 10). The analysis revealed that the calculated average mean flux was independent of the sample size (slope, t= 0.02, p = 0.98) and that the variability of the flux values remained stable between 104 and 190, around an average mean value of 156 for a sample size of about 900-1000 or higher. This supported our presumption that our sample size of 3028 for the year 2020 was sufficiently high to avoid a sample size bias in flux variability and represented a realistic system flux in the area. This high spatial
570   variability is also evident in Figure 6. Thus, it is debatable if our study area is a uniform area and if it is reasonable to average the diffusive flux for the whole study area.

y = 155.99 + 0.00015903x R^2 = 1.2636e-5
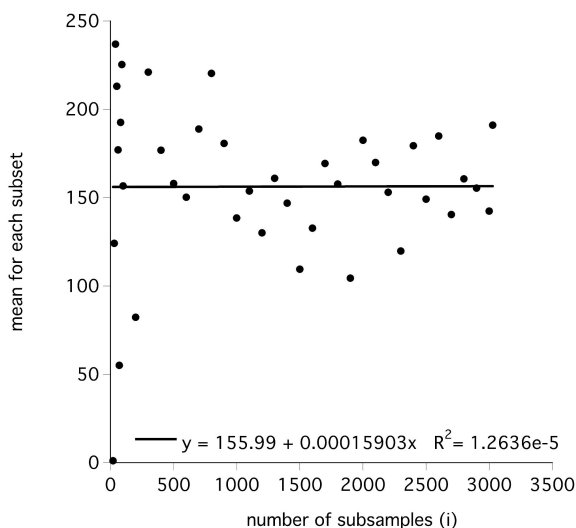
575

Figure 10: The mean of the diffusive CH₄ flux calculated for a random number of *i* subsamples. The black line indicates the regression line.

580   **4.2   Area-weighted calculation of the diffusive CH₄ flux**

To extrapolate the diffusive flux for larger areas (in mol d⁻¹), the general approach is to multiply the target area (m²) with the median or mean flux (mol d⁻¹ m⁻²) calculated from a restricted number of samples in the area. Figures S4 and S5 show the data base and frequency distribution for such a calculation for our data from the years 2019 and 2020. Both figures show a highly skewed distribution of flux values, with values <100 μmol m⁻²

585   d⁻¹ having the largest share resulting in a skewness of 3.4 and 6.1 for 2019 and 2020, respectively. Table 3 shows the results of different methods of averaging when calculating the diffusive flux for our target areas in 2019 and 2020.

According to common recommendations for data with a positive skew (data with the frequency distribution shifted to the left side), the median is always smaller than the mean (median < mean) (Köhler et al., 1996;Doane

590   and Seward, 2011). Accordingly, the median in our calculations revealed almost 3-fold lower overall flux estimates compared to the mean values. To circumvent this bias, a variety of terrestrial, marine and limnic studies (Mallast et al., 2020;Li et al., 2020;Baliña et al., 2023) stressed the importance of applying an area-weighted approach for up-scaling CO₂ flux data. We therefore also applied this method to our data (Table 3, right column). This calculation revealed that flux values for the area calculated by using the arithmetic mean are

595   identical to the area-weighted mean values and significantly higher than the median-based average flux values. In addition, the SD from the area-weighted flux was much lower. Thus, if area-weighted flux estimations are not possible due to a limited dataset, our data suggest that using the mean value is the preferred procedure rather than the median-based average flux calculations for an area.

4.3 Methane emissions from Helgoland Bay

In our study we revealed mean diffusive fluxes of 221± 351 µmol m^{-2} d^{-1} and 159 ± 444 µmol m^{-2} d^{-1} and median values of 97 and 61 µmol m^{-2} d^{-1} for 2019 and 2020, respectively

These numbers are within the same range as published previously for June 2019 (65 µmol m^{-2} d^{-1}) (Bussmann et al., 2021b). However, higher flux data are reported for autumn and winter, 104 µmol m^{-2} d^{-1} for the Dogger bank area (Mau et al., 2015) and 124–299 µmol m^{-2} d^{-1} for our study area (Winkler, 2019) (all median values). These higher fluxes were explained by the authors with higher wind velocities in the autumn / winter season. In comparison to other coastal seas our diffusive fluxes are similar to fluxes from the Belgian North Sea (161 – 221 µmol m^{-2} d^{-1} (Borges et al., 2019). In contrast much higher fluxes are reported from the Baltic Sea, with -9 – 3110 µmol m^{-2} d^{-1} by (Gutiérrez-Loza et al., 2019) and 2400 µmol m^{-2} d^{-1} by (Humborg et al., 2019). On the other side, low fluxes are reported from the Atlantic coast of Spain (7 – 20 µmol m^{-2} d^{-1}; (Ortega et al., 2023) and costal Chile (5 ± 5 µmol m^{-2} d^{-1}; (Farías et al., 2021)).

However, these comparisons are all based on the median values for the whole area. When focusing on specific locations, other patterns become evident. The lowest fluxes, i.e., negative fluxes, were observed in September 2019 in an area west of Cuxhaven (-15 to -27 µmol m^{-2} d$^{-1,}$ Fig. 4b). At this site and at this time, the water was shallow (< 5 m) with strong winds from southwest resulting in short waves. Thus, we assume that this water body was mostly depleted of CH$_4$ and was acting as CH$_4$ sink. For the open North Sea, other studies have reported undersaturation of dissolved CH$_4$ (Upstill-Goddard et al., 2000) (Bange, 2006), but not for nearshore areas like in this study.

Highest CH$_4$ concentrations were observed in the Wadden Sea and not related to river water inputs (Fig. 7). Elevated diffusive fluxes and elevated atmospheric concentrations were also observed at these locations and especially at low tide (Tab. 3). Sand flats or tidal flats are known to be a source of biogenic CH$_4$ that is released directly into the water column of the North Sea and to the atmosphere during low tide (Wu et al., 2015;Beck and Brumsack, 2012). It has been reported that peaks in CH$_4$ coincided with ebb tides at multiple sites located along the flanks of the estuary adjacent to tidal flats and wetlands (Pfeiffer-Herbert et al., 2019;Trifunovic et al., 2020). Another aspect of elevated CH$_4$ concentrations, is the distance to the coast, as described in several studies (Sierra et al., 2020) (Thomas and Borges, 2012). However, no such correlation was observed in this study; probably due to the a highly diverse coast (Wadden Sea, sandy beaches, estuaries) superimposed by tidal cycles.

4.4 Estimation of sea-air flux contribution to atmospheric concentrations

The average atmospheric CH$_4$ concentrations in this study were 2.03 ± 0.08 ppm and 2.05 ± 0.08 ppm for September 2019 and 2020, respectively. This is about 0.06 ppm higher than the values from Mace Head at the west coast of Ireland. Since 2020, there have been two new ICOS-Stations on Helgoland and Sylt, which are located in or near our study area. Their average September data (2021 and 2022) support our elevated atmospheric CH$_4$ concentrations with 2.04 ± 0.07 and 2.04 ± 0.08 ppm (Kubistin et al., 2023;Couret and Schmidt, 2023).

One aim of our study was to clarify if, or under which circumstances, the diffusive flux from the water is detectable in the atmosphere above. An increased wind speed will lead to an increased CH$_4$ flux into the

atmosphere above the water, however, this process is counteracted by the fact that increasing wind speed also leads to increased mixing of the atmosphere and any input will be quickly "diluted".

640 Our study has shown that there is only a significant correlation between CH_4 fluxes and atmospheric CH_4 concentrations at wind speeds < 5 m s^{-1}. For two examples, when we observed a strong increase of atmospheric CH_4, we estimated whether this increase was due to CH_4 input from the sea. For September 2019, the increase in atmospheric CH_4 could be attributed to the input from the sea, but not for September 2020. Thus, the static approach of (Zang et al., 2020) could not be confirmed by our data, as this approach does not take the turbulent

645 mixing of the atmosphere into account. Several other studies, which also measured atmospheric CH_4 concentrations and diffusive fluxes simultaneously, confirm this absent relationship (Myhre et al., 2016;de Groot et al., 2023;Gutiérrez-Loza et al., 2019). From our more detailed estimates, we conclude that the comparison of diffusive fluxes and atmospheric concentrations alone does not account for the interactions of diffusive flux and atmospheric convection. More insights could be obtained from inverse atmospheric modelling

650 or model-based extrapolation approaches (Saunois et al 2020; Bittig et al 2024), but are beyond the scope of this study. In future studies with further cooperation our data set might be used for these approaches.

Wind direction or advection of air masses have a strong influence on atmospheric CH_4 concentrations (Pankratova et al., 2022;Yang et al., 2019). Our data show that, when the wind was coming from the south or south-southwest, significantly higher atmospheric CH_4 concentrations were observed (2.07–2.08 ppm). Wind

655 from this direction originated from the German mainland with the ports of Bremerhaven and Wilhelmshaven, and from regions with intensive livestock farming. Our air mass origin assumptions are supported by results from the NOAA back trajectories modeling (at 10 m height, https://www.ready.noaa.gov/hypub-bin/trajasrc.pl). Air masses at the end of 3 September 2020 originated from the mainland of Lower Saxony as well as the Netherlands (Fig. S6). On the other hand, lowest atmospheric CH_4 values were observed when the wind was

660 blowing from the north (1.95 ppm) in 2019. Wind from this direction originates from the open North Sea and shows similar values as those observed at the NOAA Mace Head station in Ireland (1.965 ppm). However, in 2020, easterly winds advected low atmospheric CH_4 concentrations (1.98 ppm). These winds originated from the less populated and more agriculturally used land areas of Schleswig-Holstein, or even from the Baltic Sea. The mean wind speed of these easterly winds was 5 m s^{-1}, and the distance from Helgoland to the Baltic is about

665 200 km. Thus, the wind covered this distance within eleven hours and the air mass we were measuring could have come again from an open sea area, this time the Baltic Sea. This air mass origin is supported by the NOAA modeling, as air masses observed in our study area at the end of 1 September 2020 originated from Schleswig-Holstein and the Baltic Sea (Fig. S6).

670 ### 4.5   Conclusions

In our study we compared different methods to calculate the diffusive CH_4 fluxes with in-situ data and data from land-based meteorological stations. The usage of in-situ wind data (at high temporal resolution) was most important, while the usage of the in-situ atmospheric concentration data showed no large difference to fluxes obtained using in-situ data. When extrapolating from the measured data and from the real study area to a larger

675 area (i.e., Helgoland Bay) it was important to use the arithmetic average and not the median value. Most natural data are skewed towards the lower values, and using the median of these datasets would result in an

underestimation of diffusive CH_4 flux. The area-weighted extrapolation, however, is recommended, as it yielded the most realistic results with smallest variability.

We observed large variability in our data sets, which was not due to methodological constraints but reflects the high natural variability of the study area. Thus, it is debatable if it is reasonable to average over a heterogeneous area such as the Helgoland Bay. An improvement of flux estimates could be achieved by covering the whole area with a systematic zigzag track. New statistical methods are now available to overcome spatial and temporal restrictions of observed data sets mostly for CO_2 (Bittig et al., 2024) and their application might give new insights.

Hot spots of CH_4 emissions were the tidal flats at low tide. Their CH_4 emissions resulted in locally elevated atmospheric CH_4 concentrations. However, in shallow water and rough sea, the coastal North Sea was undersaturated with CH_4 and acted as CH_4 sink. Overall, the diffusive CH_4 flux into the atmosphere accounted for increased atmospheric CH_4 concentrations only at low wind speeds. Atmospheric advection was the main driver for low CH_4 concentrations (when coming from the sea) or high CH_4 concentrations (when coming from the mainland).

With our comprehensive study we revealed a complex relationship between dissolved CH_4 concentrations, CH_4 fluxes to the atmosphere and atmospheric CH_4 concentrations in shallow coastal water areas.

Acknowledgements: We thank the crews of our research vessels (Littorina, Ludwig Prandtl, Mya II, and Uthörn) for their support and patience. Special thanks are due to Norbert Anselm and Lea Happel for their unfailing support with our data work. Many thanks also to Jens Greinert & Tim Weiss as well as Uta Ködel for providing atmospheric CH_4 measurements on the RV Littorina and on RV Ludwig Prandtl, Mario Esposito and Felix Geissler for leading the Littorina cruises in 2029 and 2020.
This study is part of the Helmholtz program Changing Earth, subtopic 4.1: "Fluxes and transformation of energy and matter in and across compartments". We acknowledge funding from the Helmholtz Association in the framework of the Helmholtz funded observation system MOSES (Modular Observation Solutions for Earth Systems).

Author contribution: IB, HB, GF and PF planned and participated in the cruises. Data were prepared by IB and PF. IB prepared the manuscript with contributions from all co-authors.

Competing interests: NB is member of the editorial board of the journal Biogeosciences. The authors have no other competing interests to declare.

5   References

(Destatis), S. B.: Umweltökonomische Gesamtrechnung, Ökosystemgesamtrechnungen, Flächenbilanz der marinen Ökosysteme nach Nord- und Ostsee, 2021.

Ao, C. O., Waliser, D. E., Chan, S. K., Li, J.-L., Tian, B., Xie, F., and Mannucci, A. J.: Planetary boundary layer heights from GPS radio occultation refractivity and humidity profiles, Journal of Geophysical Research: Atmospheres, 117, https://doi.org/10.1029/2012JD017598, 2012.

Baliña, S., Sánchez, M. L., Izaguirre, I., and del Giorgio, P. A.: Shallow lakes under alternative states differ in the dominant greenhouse gas emission pathways, Limnol. Oceanogr., 68, 1-13, https://doi.org/10.1002/lno.12243, 2023.

Bange, H. W.: Nitrous oxide and methane in European coastal waters, Estuar. Coast. Shelf Sci., 70, 361-374, 2006.

Beck, M., and Brumsack, H. J.: Biogeochemical cycles in sediment and water column of the Wadden Sea: The example Spiekeroog Island in a regional context, Ocean and Coastal Management, 68, 102-113, 2012.

Bittig, H. C., Maurer, T. L., Plant, J. N., Schmechtig, C., Wong, A. P. S., Claustre, H., Trull, T. W., Udaya Bhaskar, T. V. S., Boss, E., Dall'Olmo, G., Organelli, E., Poteau, A., Johnson, K. S., Hanstein, C., Leymarie, E., Le Reste, S., Riser, S. C., Rupan, A. R., Taillandier, V., Thierry, V., and Xing, X.: A BGC-Argo Guide: Planning, Deployment, Data Handling and Usage, Front. Mar. Sci., 6, 10.3389/fmars.2019.00502, 2019.

Bittig, H. C., Jacobs, E., Neumann, T., and Rehder, G.: A regional pCO2 climatology of the Baltic Sea from in situ pCO2 observations and a model-based extrapolation approach, Earth Syst. Sci. Data, 16, 753-773, 10.5194/essd-16-753-2024, 2024.

Borges, A. V., Speeckaert, G. l., Champenois, W., Scranton, M. I., and Gypens, N.: Productivity and temperature as drivers of seasonal and spatial variations of dissolved methane in the Southern Bight of the North Sea, Ecosystems, DOI: 10.1007/s10021-017-0171-7, 2017.

Borges, A. V., Royer, C., Martin, J. L., Champenois, W., and Gypens, N.: Response of marine methane dissolved concentrations and emissions in the Southern North Sea to the European 2018 heatwave, Cont. Shelf Res., 190, 10.1016/j.csr.2019.104004, 2019.

Bussmann, I., Brix, H., Mario Esposito, Friedrich, M., and Fischer, P.: The MOSES Sternfahrt Expeditions of the Research Vessels LITTORINA, LUDWIG PRANDTL, MYA II, UTHÖRN to the inner German Bight in 2019, Alfred Wegener Institut, Bremerhaven, 68, 2020.

Bussmann, I., Anselm, N., Brix, H., Fischer, P., Flöser, G., Geissler, F., and Kamjunke, N.: The MOSES Sternfahrt Expeditions of the Research Vessels ALBIS, LITTORINA, LUDWIG PRANDTL, MYA II and UTHÖRN to the Elbe River, Elbe Estuary and German Bight in 2020, Alfred Wegener Institute for Polar and Marine Research, Bremerhaven, 80, 2021a.

Bussmann, I., Brix, H., Flöser, G., Ködel, U., and Fischer, P.: Detailed patterns of methane distribution in the German Bight, Front. Mar. Sci., 8, 1312, 10.3389/fmars.2021.728308, 2021b.

Couret, C., and Schmidt, M.: ICOS ATC CH4 Release, Westerland (14.0 m), 2021-07-23–2023-03-31, 2023.

de Groot, T. R., Mol, A. M., Mesdag, K., Ramond, P., Ndhlovu, R., Engelmann, J. C., Röckmann, T., and Niemann, H.: Diel and seasonal methane dynamics in the shallow and turbulent Wadden Sea, Biogeosciences, 20, 3857-3872, 10.5194/bg-20-3857-2023, 2023.

Doane, D. P., and Seward, L. E.: Measuring Skewness: A Forgotten Statistic?, Journal of Statistics Education, 19, 2011.

Dobashi, R., and Ho, D. T.: Air-sea gas exchange in a seagrass ecosystem-results from a 3Heg/gSF6 tracer release experiment, Biogeosciences, 20, 1075-1087, 10.5194/bg-20-1075-2023, 2023.

Etminan, M., Myhre, G., Highwood, E. J., and Shine, K. P.: Radiative forcing of carbon dioxide, methane, and nitrous oxide: A significant revision of the methane radiative forcing, Geophys. Res. Lett., 43, 12,614-612,623, https://doi.org/10.1002/2016GL071930, 2016.

760 Farías, L., Troncoso, M., Sanzana, K., Verdugo, J., and Masotti, I.: Spatial Distribution of Dissolved Methane Over Extreme Oceanographic Gradients in the Subtropical Eastern South Pacific (17° to 37°S), Journal of Geophysical Research: Oceans, 126, e2020JC016925, https://doi.org/10.1029/2020JC016925, 2021.

Fischer, P., Dietrich, P., Achterberg, E. P., Anselm, N., Brix, H., Bussmann, I., Eickelmann, L., Flöser, G., Friedrich, M., Rust, H., Schütze, C., and Koedel, U.: Effects of measuring devices and sampling strategies on the interpretation of monitoring data for long-term trend analysis, Front. Mar. Sci., 8,

765 10.3389/fmars.2021.770977, 2021.

Gutiérrez-Loza, L., Wallin, M. B., Sahlée, E., Nilsson, E., Bange, H. W., Kock, A., and Rutgersson, A.: Measurement of air-sea methane fluxes in the baltic sea using the eddy covariance method, Frontiers in Earth Science, 7, 10.3389/feart.2019.00093, 2019.

Gutiérrez-Loza, L., Wallin, M. B., Sahlée, E., Holding, T., Shutler, J. D., Rehder, G., and Rutgersson, A.: Air–

770 sea CO2 exchange in the Baltic Sea—A sensitivity analysis of the gas transfer velocity, J. Mar. Syst., 222, 10.1016/j.jmarsys.2021.103603, 2021.

Gutiérrez-Loza, L., Nilsson, E., Wallin, M. B., Sahlée, E., and Rutgersson, A.: On physical mechanisms enhancing air–sea CO2 exchange, Biogeosciences, 19, 5645-5665, 10.5194/bg-19-5645-2022, 2022.

Hackbusch, S., Wichels, A., and Bussmann, I.: Abundance, activity and diversity of methanotrophic bacteria in

775 the Elbe Estuary and southern North Sea, Aquat. Microb. Ecol., 83, 35-48, doi.org/10.3354/ame01899, 2019.

Ho, D. T., De Carlo, E. H., and Schlosser, P.: Air-Sea Gas Exchange and CO2 Fluxes in a Tropical Coral Reef Lagoon, Journal of Geophysical Research: Oceans, 123, 8701-8713, https://doi.org/10.1029/2018JC014423, 2018.

Humborg, C., Geibel, M. C., Sun, X., McCrackin, M., Mörth, C.-M., Stranne, C., Jakobsson, M., Gustafsson, B.,

780 Sokolov, A., Norkko, A., and Norkko, J.: High Emissions of Carbon Dioxide and Methane From the Coastal Baltic Sea at the End of a Summer Heat Wave, Front. Mar. Sci., 6, 10.3389/fmars.2019.00493, 2019.

Köhler, W., Schachtel, G., and Voleske, P.: Biostatistik, 2nd edition ed., Springer Verlag, Berlin, 1996.

Koppe, R., Gerchow, P., Macario, A., Haas, A., Schäfer-Neth, C., and Pfeiffenberger, H.: A generic framework for enabling the flow of sensor observations to archives and publications, OCEANS. 10.1109/OCEANS-

785 Genova.2015.7271657, 2015.

Kubistin, D., Plaß-Dülmer, C., Kneuer, T., Lindauer, M., and Müller-Williams, J.: ICOS ATC CH4 Release, Helgoland (110.0 m), 2020-11-17–2023-03-31, 2023.

Law, C. S., Nodder, S. D., Mountjoy, J. J., Marriner, A., Orpin, A., Pilditch, C. A., Franz, P., and Thompson, K.: Geological, hydrodynamic and biogeochemical variability of a New Zealand deep-water methane cold seep

790 during an integrated three-year time-series study, Mar. Geol., 272, 189-208, https://doi.org/10.1016/j.margeo.2009.06.018, 2010.

Li, Q., Guo, X., Zhai, W., Xu, Y., and Dai, M.: Partial pressure of CO2 and air-sea CO2 fluxes in the South China Sea: Synthesis of an 18-year dataset, Prog. Oceanogr., 182, 102272, https://doi.org/10.1016/j.pocean.2020.102272, 2020.

795   Magen, C., Lapham, L. L., Pohlman, J. W., Marshall, K., Bosman, S., Casso, M., and Chanton, J. P.: A simple headspace equilibration method for measuring dissolved methane, Limnol. Oceanogr.: Methods, 12, 637-650, doi:10.4319/lom.2014.12.637, 2014.

Mallast, U., Staniek, M., and Koschorreck, M.: Spatial upscaling of CO_2 emissions from exposed river sediments of the Elbe River during an extreme drought, Ecohydrology, 13, e2216,

800   https://doi.org/10.1002/eco.2216, 2020.

Matousu, A., Osudar, R., Simek, K., and Bussmann, I.: Methane distribution and methane oxidation in the water column of the Elbe estuary, Germany, Aquat. Sci., 79, 443-458, 10.1007/s00027-016-0509-9, 2017.

Mau, S., Gentz, T., Körber, J. H., Torres, M. E., Römer, M., Sahling, H., Wintersteller, P., Martinez, R., Schlüter, M., and Helmke, E.: Seasonal methane accumulation and release from a gas emission site in the

805   central North Sea, Biogeosciences, 12, 5261-5276, doi:10.5194/bg-12-5261-2015, 2015.

Myhre, C. L., Ferré, B., Platt, S. M., Silyakova, A., Hermansen, O., Allen, G., Pisso, I., Schmidbauer, N., Stohl, A., Pitt, J., Jansson, P., Greinert, J., Percival, C., Fjaeraa, A. M., O'Shea, S. J., Gallagher, M., Breton, M. L., Bower, K. N., Bauguitte, S. J. B., Dalsøren, S., Vadakkepuliyambatta, S., Fisher, R. E., Nisbet, E. G., Lowry, D., G.Myhre, Pyle, A., Cain, M., and Mienert, J.: Extensive release of methane from Arctic seabed west of

810   Svalbard during summer 2014 does not influence the atmosphere, Geophys. Res. Lett., 43, 4624–4631, doi:10.1002/2016GL068999, 2016.

Myllykangas, J.-P., Hietanen, S., and Jilbert, T.: Legacy Effects of Eutrophication on Modern Methane Dynamics in a Boreal Estuary, Estuaries and Coasts, 43, 189-206, 10.1007/s12237-019-00677-0, 2020.

Nightingale, P. D., Malin, G., Law, C. S., Watson, A. J., Liss, P. S., Liddicoat, M. I., Boutin, J., and Upstill-

815   Goddard, R. C.: In situ evaluation of air-sea gas exchange parameterizations using novel conservative and volatile tracers, Glob. Biogeochem. Cycl., 14, 373-387, doi:10.1029/1999GB900091, 2000.

Ortega, T., Jiménez-López, D., Sierra, A., Ponce, R., and Forja, J.: Greenhouse gas assemblages (CO_2, CH_4 and N_2O) in the continental shelf of the Gulf of Cadiz (SW Iberian Peninsula), Sci. Total Environ., 898, 165474, https://doi.org/10.1016/j.scitotenv.2023.165474, 2023.

820   Osudar, R., Matoušů, A., Alawi, M., Wagner, D., and Bussmann, I.: Environmental factors affecting methane distribution and bacterial methane oxidation in the German Bight (North Sea), Estuar. Coast. Shelf Sci., 160, 10-21, doi:10.1016/j.ecss.2015.03.028, 2015.

Pankratova, N. V., Belikov, I. B., Skorokhod, A. I., Belousov, V. A., Muravya, V. O., Flint, M. V., Berezina, E. V., and Novigatsky, A. N.: Methane Concentration and $\delta 13C$ Isotopic Signature in Methane over Arctic Seas in

825   Summer and Autumn 2020, Oceanology, 62, 757-764, 10.1134/S0001437022060108, 2022.

Petersen, W.: FerryBox systems: State-of-the-art in Europe and future development, J. Mar. Syst., 140, 4-12, 10.1016/j.jmarsys.2014.07.003, 2014.

Pfeiffer-Herbert, A. S., Prahl, F. G., Peterson, T. D., and Wolhowe, M.: Methane Dynamics Associated with Tidal Processes in the Lower Columbia River, Estuaries and Coasts, 10.1007/s12237-019-00568-4, 2019.

830   Römer, M., Blumenberg, M., Heeschen, K., Schloemer, S., Müller, H., Müller, S., Hilgenfeldt, C., Barckhausen, U., and Schwalenberg, K.: Seafloor Methane Seepage Related to Salt Diapirism in the Northwestern Part of the German North Sea, Frontiers in Earth Science, 9, 10.3389/feart.2021.556329, 2021.

Rosentreter, J. A., Borges, A. V., Deemer, B. R., Holgerson, M. A., Liu, S., Song, C., Melack, J., Raymond, P. A., Duarte, C. M., Allen, G. H., Olefeldt, D., Poulter, B., Battin, T. I., and Eyre, B. D.: Half of global methane

emissions come from highly variable aquatic ecosystem sources, Nature Geoscience, 14, 225-230, 10.1038/s41561-021-00715-2, 2021a.

Rosentreter, J. A., Wells, N. S., Ulseth, A. J., and Eyre, B. D.: Divergent Gas Transfer Velocities of CO2, CH4, and N2O Over Spatial and Temporal Gradients in a Subtropical Estuary, Journal of Geophysical Research: Biogeosciences, 126, 10.1029/2021JG006270, 2021b.

Røy, H., Jae, S. L., Jansen, S., and De Beer, D.: Tide-driven deep pore-water flow in intertidal sand flats, Limnol. Oceanogr., 53, 1521-1530, 2008.

Saunois, M., Stavert, A. R., Poulter, B., Bousquet, P., Canadell, J. G., Jackson, R. B., Raymond, P. A., Dlugokencky, E. J., Houweling, S., Patra, P. K., Ciais, P., Arora, V. K., Bastviken, D., Bergamaschi, P., Blake, D. R., Brailsford, G., Bruhwiler, L., Carlson, K. M., Carrol, M., Castaldi, S., Chandra, N., Crevoisier, C., Crill, P. M., Covey, K., Curry, C. L., Etiope, G., Frankenberg, C., Gedney, N., Hegglin, M. I., Höglund-Isaksson, L., Hugelius, G., Ishizawa, M., Ito, A., Janssens-Maenhout, G., Jensen, K. M., Joos, F., Kleinen, T., Krummel, P. B., Langenfelds, R. L., Laruelle, G. G., Liu, L., Machida, T., Maksyutov, S., McDonald, K. C., McNorton, J., Miller, P. A., Melton, J. R., Morino, I., Müller, J., Murguia-Flores, F., Naik, V., Niwa, Y., Noce, S., O'Doherty, S., Parker, R. J., Peng, C., Peng, S., Peters, G. P., Prigent, C., Prinn, R., Ramonet, M., Regnier, P., Riley, W. J., Rosentreter, J. A., Segers, A., Simpson, I. J., Shi, H., Smith, S. J., Steele, L. P., Thornton, B. F., Tian, H., Tohjima, Y., Tubiello, F. N., Tsuruta, A., Viovy, N., Voulgarakis, A., Weber, T. S., van Weele, M., van der Werf, G. R., Weiss, R. F., Worthy, D., Wunch, D., Yin, Y., Yoshida, Y., Zhang, W., Zhang, Z., Zhao, Y., Zheng, B., Zhu, Q., Zhu, Q., and Zhuang, Q.: The Global Methane Budget 2000–2017, Earth Syst. Sci. Data, 12, 1561-1623, 10.5194/essd-12-1561-2020, 2020.

Sierra, A., Jiménez-López, D., Ortega, T., Fernández-Puga, M. C., Delgado-Huertas, A., and Forja, J.: Methane dynamics in the coastal – Continental shelf transition zone of the Gulf of Cadiz, Estuar. Coast. Shelf Sci., 236, 10.1016/j.ecss.2020.106653, 2020.

Silyakova, A., Jansson, P., Serov, P., Ferré, B., Pavlov, A. K., Hattermann, T., Graves, C. A., Platt, S. M., Myhre, C. L., Gründger, F., and Niemann, H.: Physical controls of dynamics of methane venting from a shallow seep area west of Svalbard, Cont. Shelf Res., 194, 10.1016/j.csr.2019.104030, 2020.

Striegl, R. G., Dornblaser, M. M., McDonald, C. P., Rover, J. R., and Stets, E. G.: Carbon dioxide and methane emissions from the Yukon River system, Glob. Biogeochem. Cycl., 26, doi:10.1029/2012GB004306, 2012.

Thomas, H., and Borges, A. V.: Biogeochemistry of coastal seas and continental shelves – Including biogeochemistry during the International Polar Year, Estuar. Coast. Shelf Sci., 100, 1-2, https://doi.org/10.1016/j.ecss.2012.02.016, 2012.

Touma, J. S.: Dependence of the wind profile power law on stability for various locations J. Air Pollution Control Association, 27, 863-866, 1977.

Trifunovic, B., Vázquez-Lule, A., Capooci, M., Seyfferth, A. L., Moffat, C., and Vargas, R.: Carbon Dioxide and Methane Emissions From A Temperate Salt Marsh Tidal Creek, Journal of Geophysical Research: Biogeosciences, 125, e2019JG005558, https://doi.org/10.1029/2019JG005558, 2020.

Upstill-Goddard, R. C., Barnes, J., and Owens, N. J. P.: Methane in the southern North Sea: Low-salinity inputs, estuarine removal, and atmospheric flux, Glob. Biogeochem. Cycl., 14, 1205, 2000.

Upstill-Goddard, R. C., and Barnes, J.: Methane emissions from UK estuaries: Re-evaluating the estuarine source of tropospheric methane from Europe, Mar. Chem., 180, 14-23, 10.1016/j.marchem.2016.01.010, 2016.

875 Vielstädte, L., Haeckel, M., Karstens, J., Linke, P., Schmidt, M., Steinle, L., and Wallmann, K.: Shallow Gas Migration along Hydrocarbon Wells-An Unconsidered, Anthropogenic Source of Biogenic Methane in the North Sea, Environ. Sci. Technol., 51, 10262-10268, 10.1021/acs.est.7b02732, 2017.

Vogt, J., Risk, D., Bourlon, E., Azetsu-Scott, K., Edinger, E. N., and Sherwood, O. A.: Sea–air methane flux estimates derived from marine surface observations and instantaneous atmospheric measurements in the

880 northern Labrador Sea and Baffin Bay, Biogeosciences, 20, 1773-1787, 10.5194/bg-20-1773-2023, 2023.

Wanninkhof, R., Asher, W. E., Ho, D. T., Sweeney, C. S., and McGillis, W. R.: Advances in quantifying air-sea gas exchange and environmental forcing, Annual Review of Marine Science (2009), 1, 213-244, doi:10.1146/annurev.marine.010908.163742, 2009.

Wanninkhof, R.: Relationship between wind speed and gas exchange over the ocean revisited, Limnol.

885 Oceanogr.: Methods, 12, 351-362, doi:10.4319/lom.2014.12.351, 2014.

Weber, T., Wiseman, N. A., and Kock, A.: Global ocean methane emissions dominated by shallow coastal waters, Nature Communications, 10, 10.1038/s41467-019-12541-7, 2019.

Weber, U., Attinger, S., Baschek, B., Boike, J., Borchardt, D., Brix, H., Brüggemann, N., Bussmann, I., Dietrich, P., Fischer, P., Greinert, J., Hajnsek, I., Kamjunke, N., Kerschke, D., Kiendler-Scharr, A., Körtzinger,

890 A., Kottmeier, C., Merz, B., Merz, R., Riese, M., Schloter, M., Schmid, H., Schnitzler, J. P., Sachs, T., Schütze, C., Tillmann, R., Vereecken, H., Wieser, A., and Teutsch, G.: MOSES: A Novel Observation System to Monitor Dynamic Events Across Earth Compartments ,, Bulletin of the American Meteorological Society, 1-23, doi:10.1175/BAMS-D-20-0158.1, 2021.

Wiesenburg, D. A., and Guinasso, N. L.: Equilibrium solubilities of methane, carbon monoxide and hydrogen in

895 water and sea water, J. Chem. Eng. Data, 24, 356-360, 1979.

Winkler, H.: High resolution methane measurements and impacts of environmental factors on the methane distribution in the Elbe Estuary, University of Vienna, 2019.

Woszczyk, M., and Schubert, C. J.: Greenhouse gas emissions from Baltic coastal lakes, Sci. Total Environ., 755, 143500, https://doi.org/10.1016/j.scitotenv.2020.143500, 2021.

900 Wu, C. S., Røy, H., and de Beer, D.: Methanogenesis in sediments of an intertidal sand flat in the Wadden Sea, Estuar. Coast. Shelf Sci., 164, 39-45, http://dx.doi.org/10.1016/j.ecss.2015.06.031, 2015.

Yang, M., Bell, T. G., Brown, I. J., Fishwick, J. R., Kitidis, V., Nightingale, P. D., Rees, A. P., and Smyth, T. J.: Insights from year-long measurements of air–water CH4 and CO2 exchange in a coastal environment, Biogeosciences, 16, 961-978, 10.5194/bg-16-961-2019, 2019.

905 Yin, X., Wu, W., Maeke, M., Richter-Heitmann, T., Kulkarni, A. C., Oni, O. E., Wendt, J., Elvert, M., and Friedrich, M. W.: CO2 conversion to methane and biomass in obligate methylotrophic methanogens in marine sediments, ISME Journal, 13, 2107-2119, 10.1038/s41396-019-0425-9, 2019.

Zang, K., Zhang, G., Xu, X., and Yao, Z.: Impact of air-sea exchange on the spatial distribution of atmospheric methane in the Dalian Bay and adjacent coastal area, China, Chemosphere, 251,

910 10.1016/j.chemosphere.2020.126412, 2020.

hat gelöscht: ¶
¶
¶
Supplement¶
¶
Hydrographic parameters:¶
In the RV Ludwig Prandtl, the built-in FerryBox (Petersen, 2014) recorded data using a Teledyne RDI thermosalinograph (temperature and salinity), Aanderaa oxygen optode 4330(oxygen concentration and saturation), Meinsberg pH electrode (pH values), and SCUFA submersible chlorophyll fluorometer (turbidity and fluorescence). The data were stored on board and automatically sent via a mobile phone connection to the Hereon database. The water flow in the FerryBox was approximately 12 L min/1. In the RV Mya II, the built in Ferrybox recorded data using a salinometer (FSI), and SBE38 Digital Oceanographic Thermometer (SBE38) for salinity and temperature. For pH measurements a Meinsberg pH Sensor was used and for oxygen an Aanderaa oxygen optode. On the RV Uthörn and RV Littorina, a portable pocket FerryBox (4HJena, Germany) was used to record the hydrographic parameters using the following sensors: Seabird SBE45 thermosalinograph, Aanderaa oxygen optode, Meinsberg pH electrode, Seapoint Chlorophyll Fluorometer (SCF), and Seapoint Turbidity Meter. The water flow was between 3 and 4 L min/1. Data were saved once per minute.¶
¶
¶
¶
¶
¶